Phase Relations in the Cu-In-S System and Growth of Large $CuInS_2$ Single Crystals

M. L. Fearheiley,* N. Dietz, and H. J. Lewerenz*

Hahn-Meitner-Institut, Bereich Strahlenchemie, Glienicker Strasse 100, 1000 Berlin 39, Germany

ABSTRACT

The phase relations in the metal portion of the Cu-In-S system have been investigated by differential thermal analysis (DTA) and x-ray diffraction (XRD). The Cu-$CuInS_2$ pseudobinary reveals a region of liquid immiscibility indicating the extension of the two liquid region from the Cu-S binary to the In-S binary. This two liquid region is intersected by two eutectics which originate at the Cu_2S-In_2S_3 quasibinary system. In addition, the growth of large single crystals of $CuInS_2$ have been facilitated by growth under elevated argon pressures. Growth in large temperature gradients results in a lamellar type phase, which shows good optical and electrical properties. Data from XRD, reflection high energy electron diffraction, and rocking curves are presented on the structural and morphological properties, and photoluminescence was used for a defect characterization of this material.

$CuInS_2$ has received attention as a possible alternative base material for solar cells (1-15). At room temperature $CuInS_2$ has the chalcopyrite structure and possesses a bandgap of 1.55 eV, which lies near the optimum for homojunction solar cell devices (16). The first highly photoactive material in a non-optimum configuration has been reported from our laboratory (3). Recently, a thin film device has been produced exhibiting a 7.3% power conversion efficiency (5).

With regards to the phase relations, the binaries Cu-In (17), Cu-S (18), and In-S (19) have been previously investigated. Both the Cu-S and In-S binaries exhibit large regions of liquid immiscibility which are expected to influence the liquidus in the ternary system (Fig. 1). The compounds Cu_2S and In_2S_3 are both congruently melting and form a quasibinary system in the ternary. This quasibinary contains the spinel $CuIn_5S_8$ as well as $CuInS_2$, which was found to melt congruently at 1090°C and undergo two solid state phase transformations (20). The Cu-In binary contains several intermetallic compounds. The liquidus for the system $Cu_{0.5}In_{0.5}$-$CuInS_2$ (21) revealed a region of liquid immiscibility. The overall phase relations at room temperature were determined by a nuclear probe method (22, 23). Differential thermal analysis (DTA) and x-ray powder diffraction were the primary methods used in establishing the phase relations for the Cu-$CuInS_2$ pseudobinary system.

For applications in high efficiency energy converting systems, such as concentrators, the growth of high quality single crystalline material is mandatory. With a direct energy gap (E_g = 1.54 eV) in the optimum range of the theoretical solar conversion efficiency a minority carrier diffusion length of about 2 μm would be sufficient for effective carrier collection in the relevant spectral range (24, 25).

The performance of $CuInS_2$ solar cells has lagged behind that of its selenide analog, whose current efficiency is around 14%. Among the differences in material preparation of the sulfide and selenide chalcopyrite is the significant variation of the chalcogenide vapor pressure. Due to the higher vapor pressure of sulfur, similar growth conditions as for $CuInSe_2$ can only be expected for growth in an inert atmosphere at elevated pressure, as this reduces the sulfur partial pressure.

In this paper we describe for the first time the growth of $CuInS_2$ in an argon atmosphere at about 25 bar at the melting point, using a two-zone gradient freeze technique. We present data on the structural and morphological properties, and perform a defect analysis.

Experimental

DTA.—$CuInS_2$ powder, obtained from material synthesized by the two-zone gradient freeze method (26), and (99.999%) In or Cu were used for the DTA studies. The $CuInS_2$ starting material was analyzed by room temperature x-ray diffraction, DTA, and electron probe microanalysis to establish its homogeneity and stoichiometry and was found to represent the desired material with little variation of the composition.

Samples of predetermined amounts of In or Cu and $CuInS_2$ were sealed under vacuum in 5 mm quartz tubes and placed in platinum crucibles to ensure a uniform temperature. The temperature programming and data acquisition were performed by use of a Netzsch Simultaneous Thermal Analyser 409. Heating and cooling runs were conducted at rates from 2 to 10°C/min with the rate 5°C/min chosen for the present study.

XRD.—Powder diffractograms were measured in the usual θ-2θ-coupled geometry with a SIEMENS D500, using a Cu-anode with 45 kV and 30 mA. A secondary graphite monochromator was used to avoid Kβ-reflections and to reduce fluorescent scattering (λ(CuKα) = 1.5418 Å). All measurements were done in a step scan mode ($x°/y$ sec).

Crystal growth.—The gradient freeze technique (26) was used to grow $CuInS_2$ single crystals. A thick-walled quartz ampul containing the reactants was evacuated and refilled twice with argon, and the third argon fill was condensed using liquid nitrogen. The resulting argon pressure in the ampul was calculated to be around 5 bar at room temperature. A two zone oven was used for the growth experiments in order to independently control the temperature of the metals and sulfur. The Cu/In zone was heated to a temperature of 800°C, then the sulfur zone was heated to

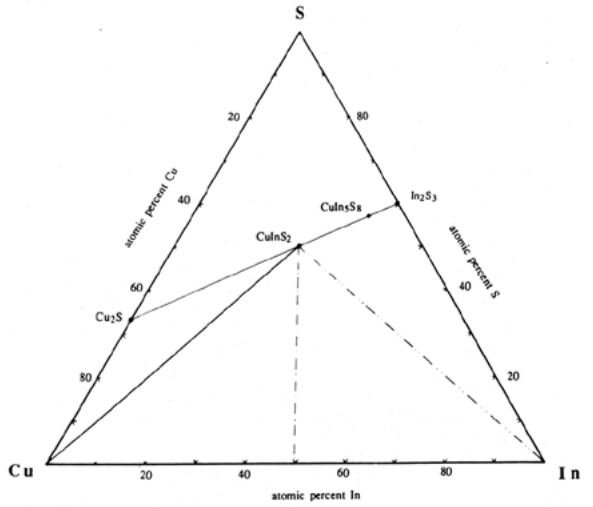

Fig. 1. The Cu-In-S ternary system. The Cu_2S-In_2S_3 quasibinary (20), the $Cu_{0.5}In_{0.5}$-S (21), and the In-$CuInS_2$ (27) pseudobinaries have previously been investigated. Information concerning the Cu-$CuInS_2$ pseudobinary is presented here.

* Electrochemical Society Active Member.

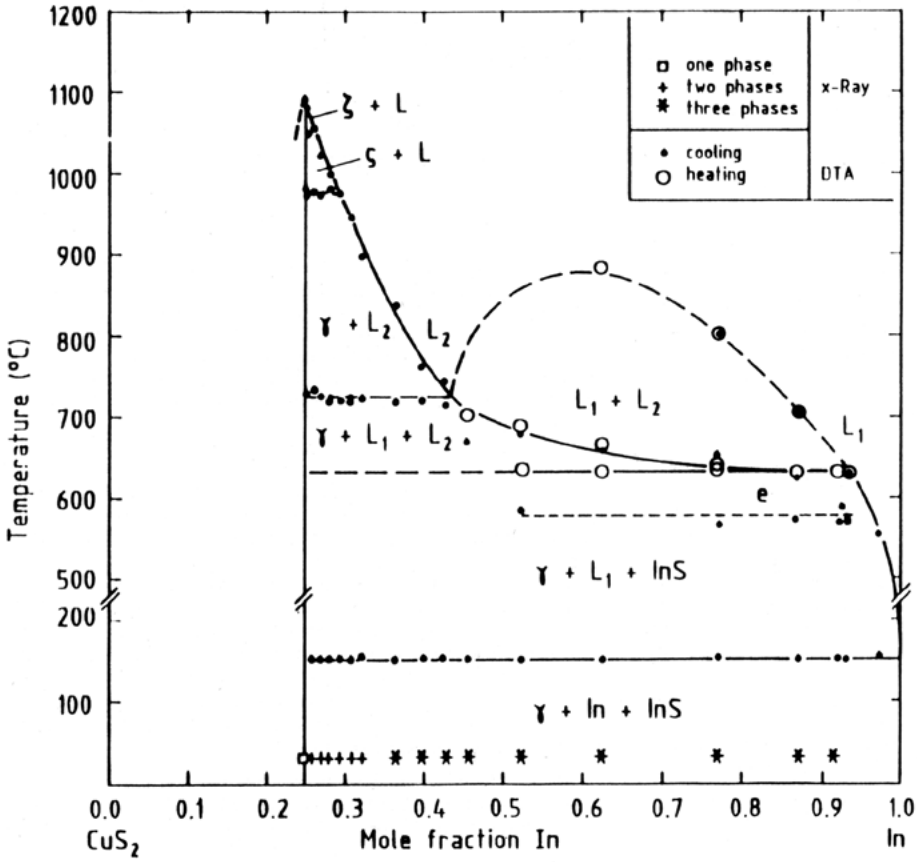

Fig. 2. The In-$CuInS_2$ pseudobinary system.

450°C at a rate of between 50 and 100°C/h. After the constituents had reacted, the temperature of both zones was raised to 1100°C at a rate of 50°C/h. At this temperature the argon pressure is approximately 25 bar. The melt was allowed to homogenize for approximately 21 h, then cooled at a rate from 1 to 5°C/h through the melting point (1090°C), then quickly cooled to the next transition point (1045°C), where the rate was once again reduced to 1 to 5°C/h. This was repeated a third time at 980°C, then cooled to room temperature.

The amount of the starting material remained the same as the position of the boat was varied in the temperature gradient. This gradient ranged from 2 to 15°C/cm and experiments without an argon overpressure were also done. The growth runs resulted in two different surface morphologies.

RHEED.—The beam energy of the impinging electrons was 90 keV and at an angle of 2° the penetration depth was approximately 10 Å.

Rocking curve.—Rocking curves were recorded with a wavelength of 0.0392 Å having a resolution of three minutes.

PL.—PL measurements were performed as a function of temperature by using an Excimer laser to pump a Dye laser. The excitation wavelength was 540 nm, the beam power was 18 mW. The samples were mounted into a TIC 303M continuous flow liquid helium cryostat. The emission spectra were recorded using a Spex 1401 monochrometer with a resolution of 2 meV and an S1 photomultiplier detector.

Results and Discussion

The In-$CuInS_2$ pseudobinary.—The pseudobinary $CuInS_2$-In (27) is reproduced in Fig. 2. Our results for the transitions of stoichiometric $CuInS_2$ agree reasonably well with those of Binsma *et al.* (20). $CuInS_2$ was found to melt at 1090°C (1090°C) with solid state phase transformations occurring at 1047 (1045°C) and 975°C (980°C). The wurtzite and zinc blende high temperature modifications, ζ and δ, were not stabilized with respect to the chalcopyrite, γ-phase with excess In. Nor was there appreciable solubility of In in $CuInS_2$. The two liquid region extends from $X_{In} = 0.43$ to approximately $X_{In} = 0.93$ and has a critical temperature along this pseudobinary at approximately 845°C. Due to undercooling of the melt, the formation of InS, as well as the formation of γ (but less severely), occurs at lower temperatures and the metastable invariant reaction was found to take place at around 580°C. This phenomenon was also encountered in the study of the In_xS_{1-x} system (19). X-ray powder diffraction analysis of the resulting DTA samples containing a large In express clearly showed the presence of red InS crystals. This would indicate the existence of the $L_2 = L_1 + InS$ reaction along this pseudobinary as well as the $L_2 = L_1 + \gamma$ reaction. The monotectic reactions reach a minimum at the invariant reaction temperature of 633°C. The reaction at this eutectic would therefore be $L_2 = L_1 + \gamma + InS$ with the eutectic crossing this pseudobinary between $X_{In} = 0.85$ to 0.90 In, or *e* in Fig. 2. We were not able to resolve the location of this eutectic due to the close proximity of the isotherm and the monotectic on the In-rich side. The liquidus beyond the monotectic ends at a degenerate eutectic near the indium corner at a temperature of 153°C.

The Cu-$CuInS_2$ pseudobinary.—Results obtained by DTA for the Cu-$CuInS_2$ pseudobinary are given in Fig. 3. The main feature is the two liquid region, $L_1 + L_2$. Its boundaries are given by two DTA peaks which are characteristic for liquid separation. These were found at $X_{Cu} = 0.97$ (1130°C) and $X_{Cu} = 0.45$ (795°C). Below this two liquid region L_2 decomposes to a solid, and, in this case, into one of two different solids depending on the Cu concentration. On the Cu side the reaction $L_2 = L_1 + Cu_2S$ is found; on the $CuInS_2$ side the reaction $L_2 = L_1 + CuInS_2$ occurs. These two regions meet at the eutectic ($X_{Cu} = 0.55$, 720°C), where the four phase invariant reaction proceeds. L_1 is completely consumed at the thermal arrests found at 675°C. Below this point the phase relations become more complicated to decipher.

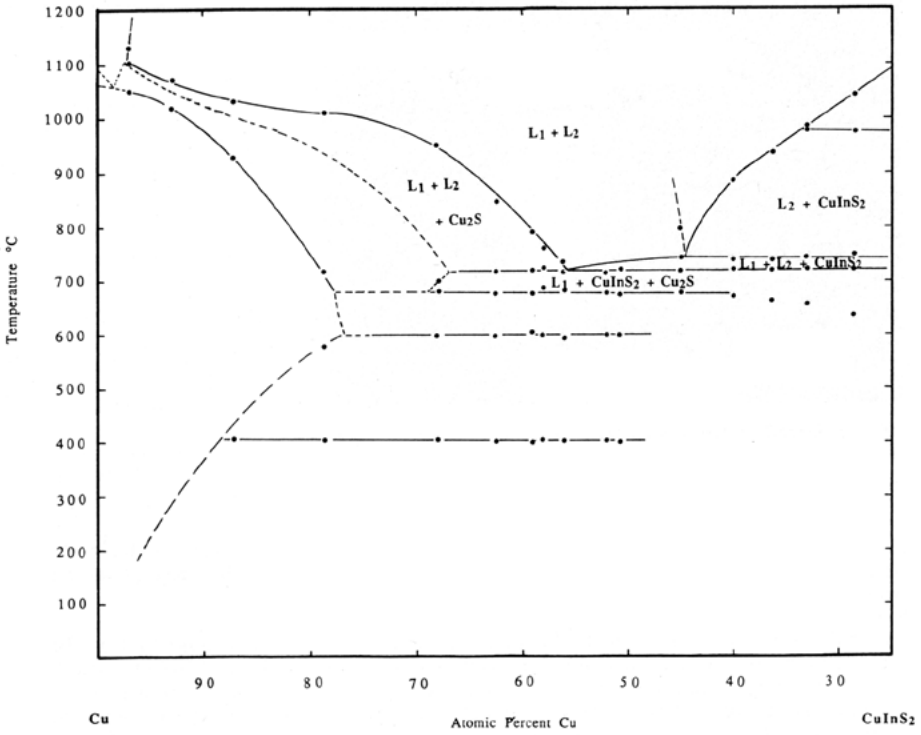

Fig. 3. The $Cu\text{-}CuInS_2$ pseudobinary system.

X-ray analysis of the end samples revealed Cu and $CuInS_2$ as the major constituents. Cu_2S was present only in minor amounts, but this is probably due to the rate of cooling. The components in the solid were not able to completely react, leaving traces of Cu_2S in the end product. For that reason, the reaction at 400°C (Fig. 3) is believed to be the formation of $\beta\text{-}Cu_2S$. This is supported by the fact that the thermal arrests are weak and are found extending little past the eutectic composition, where Cu_2S is not formed.

Regarding the transition at 600°C and the sub-solidus near the Cu-rich compositions, little can be said. The $L_1 + Cu_2S$ phase field should be bound by the $L_1 + Cu_2S + Cu$ three-phase field, however, little could be established by DTA. High temperature x-ray would have to be used.

The liquidus isotherm projection.—Combining this information with that previously referenced, a liquidus isothermal projection has been constructed (Fig. 4). The liquidus around $CuInS_2$ is stretched along the $Cu_2S\text{-}In_2S_3$ axis. The two eutectics, e_1 and e_2, descend from this quasibinary and pass through the two liquid region, $L_1 + L_2$. The points indicated in the figure are for the isotherms and not necessarily points investigated by DTA. It is assumed that the eutectic at $Cu_{98.5}S_{1.5}$ becomes degenerated with the Cu-In binary near the peritectic. With regard to preliminary work on the $Cu_{9x}In_{9(1-x)}S_1$ pseudobinary (not shown), the close correspondence between the thermal arrests below the monotectic and those of the Cu-In binary, it is likely that there is little sulfur solubility in L_1, therefore the two liquid boundary is drawn close to the Cu-In binary.

Structural analysis.—By using an argon overpressure (25 bar at the melting point) during the growth of $CuInS_2$ from its melt, we were able to grow large, single crystals. This process led to two types of crystals, depending on the temperature gradient above the liquid/melt interface. For relatively moderate temperature gradients single crystals on the order of $10 \times 10 \times 3$ mm^3 were obtained. For steeper temperature gradients crystals possessing a lamellar type structure were obtained (Fig. 5). Surprisingly, both types of samples could be easily cleaved, which is not expected for a chalcopyrite structure. The comparison of Debye Scherrer diffraction data with file data shows both materi-

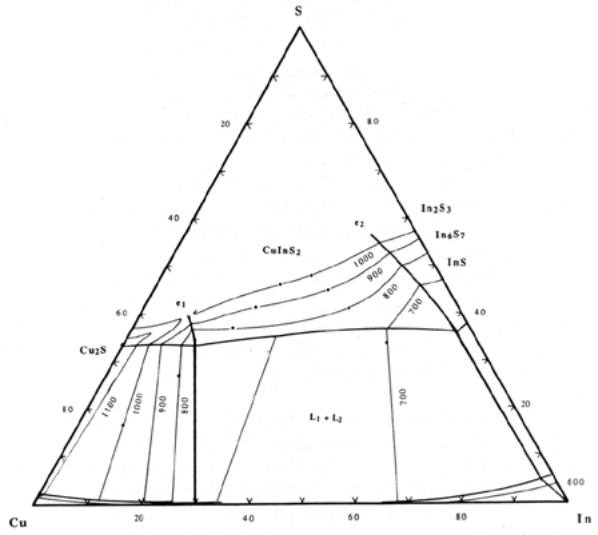

Fig. 4. The liquidus isotherm projection for the system Cu-In-S.

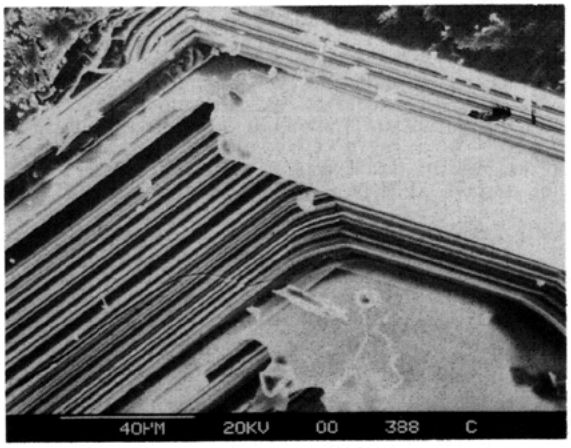

Fig. 5. Scanning electron micrograph of the lamellar-type material.

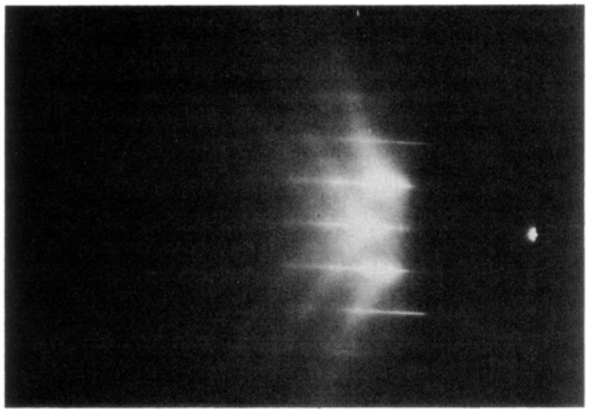

Fig. 6. RHEED pattern arising from the <112> planes of $CuInS_2$ lamellar type material. A beam energy of 90 keV was used at an angle of 2° with a penetration depth of approximately 10 Å.

als to be single phase $CuInS_2$ within the experimental limitations of the method. Foreign phases with a volume contribution below 2% cannot easily be detected. This problem will be addressed later. The lattice constants inferred from the data are $a = 5.760$ Å, and $c = 11.50$ Å. Laue diffraction pattern obtained from a cleaved sample show <112> orientation, an indication that cleavage occurs predominantly along <112> planes. The natural cleavage planes for $CuInS_2$ are <110> orientated (28, 29). The quality of the crystals can be seen most readily from x-ray and electron microscopic analyses. The observance of Kikuchi lines, Fig. 6, requires near perfection of the crystals, otherwise defects would spread these lines over larger angles. The data confirm the <112> orientation of the cleavage planes. The occurrence of Kikuchi lines demonstrates quite high crystallinity over extended regions of the sample. The lattice constant determined from the RHEED experiment is $a = 5.76$ Å with $c/a = 2.04$.

Shown in Fig. 7 is a rocking curve which was performed to determine the relative dislocation density. The FWHM of 1140 seconds is indicative of a structure containing substantial amounts of dislocations, possibly also microscrystalites. For comparison, data for GaAs (30) grown in a contaminated environment are shown in the inset. The $CuInS_2$ crystal is characterized by a FWHM which is approximately 6 times larger than that for GaAs. It should be noted that the room temperature homogeneity range is substantially different for GaAs and $CuInS_2$. In fact, the extension of the homogeneity range of $CuInS_2$ is not exactly known at present. The influence of modification of growth parameters on the structural characteristic has also been investigated.

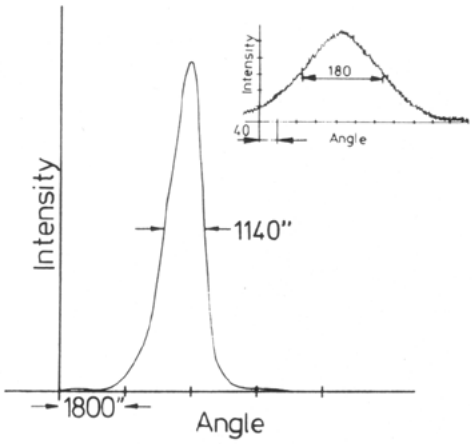

Fig. 7. Rocking curve for the <112> reflection. Inset: rocking curve for GaAs <111> grown in a contaminated environment (30).

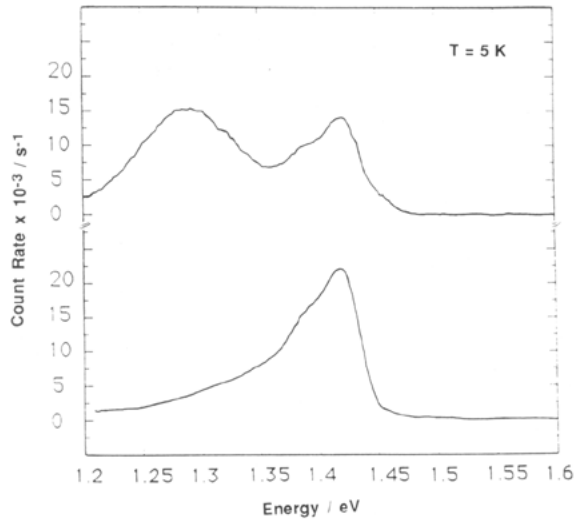

Fig. 8. PL spectra at 5 K for the two types of $CuInS_2$ crystals. Bottom: lamellar-type structure; top: single crystal.

Although x-ray diffraction and electron microprobe showed the material to be $CuInS_2$, within their respective limits, the material exhibited, for instance, a different mechanical behavior compared to the expected one for $CuInS_2$. The material could be cleaved, and very thin layers could be pealed off with adhesive tape, similar to the procedures known for layered crystals like WSe_2. An analysis of the <112> planes after cleavage in vacuo by XPS revealed large deviations of the Cu to In ratio from 1 (31). The penetration depth is of the order of ten atomic layers and the fact that the Cu to In ratio is not consistent on both cleaved surfaces means the second phase is probably only a few atomic layers thin, less than the penetration depth. This second phase could have formed during freezing due to the stressed environment brought about by the steep temperature gradient and/or high pressures. The nature of this phase is currently under investigation.

Optical properties.—The PL spectra of the two sample types investigated are compared in Fig. 8. The spectrum in 8(a) represents single crystal $CuInS_2$ and exhibits the well known broad band emission at about 1.3 eV (32, 33) and a broadened signal between 1.38 and 1.42 eV. The low energy structure has also been found in sub bandgap photoresponse measurements (32) and can be attributed to sulfur excess. The energetically higher signal is typical for Cu-rich samples, although the shoulder located by 0.04 eV towards lower energy is somewhat less pronounced than in the data presented by Binsma (34, 35).

The signal from the lamellar-type material in Fig. 8(b) shows some similarity with the so-called optimized samples of high photoactivity (3) although the features here are more blurred and the peak position corresponds rather to Cu-rich materials than to samples with In excess. The missing low energy emission, however, indicates a somewhat increased electronic quality of these samples.

Figure 9 displays the temperature dependence of the luminescence signal of lamellar structured samples. A pronounced shift is observed for temperatures ranging from 5 to 150 K. The energetic difference in the main structure (peak at 1.42 eV and shoulder at 1.38 eV at 5 K) remains unaffected by temperature. The structure at $h\nu = 1.35$ eV which is almost absent at 5 K becomes more pronounced with increased temperature but stays invariant in energetic position.

The interpretation of the data in Fig. 9 and 10 has to take into account that the bandgap of $CuInS_2$ increases with temperature up to 80 K and then decreases. The temperature coefficient dE/dT, deduced from the peak shift, varies between 2.7×10^{-5} and 4.6×10^{-5} eV K^{-1} and corresponds quite well to published data (33). This behavior is usually interpreted as donor to accepter transition, in which the

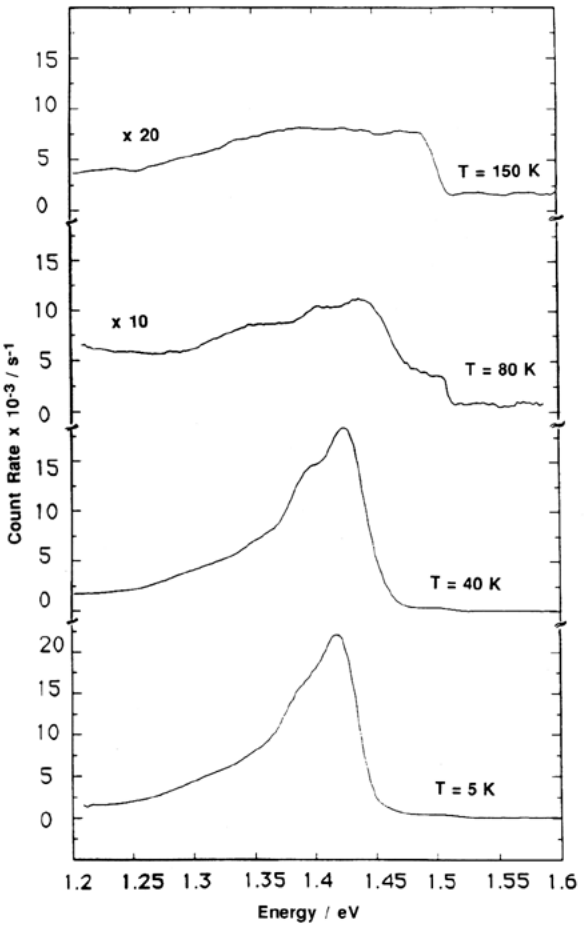

Fig. 9. Temperature dependence of the PL spectra for the lamellar-type structure.

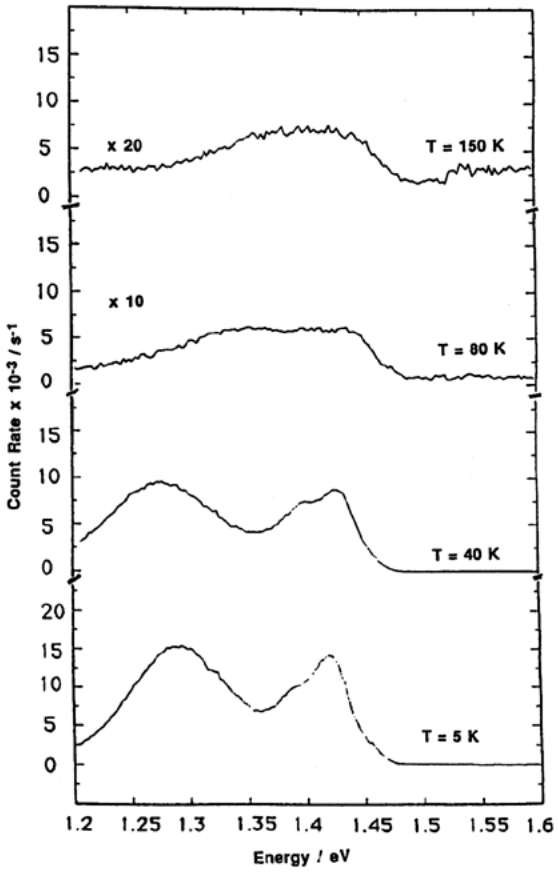

Fig. 10. Temperature dependence of the PL for the single crystal.

peak energy shows a more rapid increase with temperature than the bandgap energy. With $h\nu_p = E_g - E_A - E_D + e^2/\epsilon r$ and a variation in E_g between 5 and 80 K of ~3 meV and $\Delta E_g = -3$ meV between 80 and 150 K, the increase of $h\nu_p$ with temperature indicates a more pronounced decrease of the Coulomb term in the equation due to increased mobility with temperature and therefore decreasing radii r. The higher temperature coefficient of 4.6×10^{-5} eV K^{-1} between 80 and 150 K, might also indicate the contribution of transitions involving a band (free to bound emission) which makes the interpretation difficult (33).

Conclusions

The phase relations in the metal rich-portion of the Cu-In-S system was reported. Revealed on the Cu-$CuInS_2$ pseudobinary cut was a broad region of liquid immiscibility. This indicates that this region of liquid immiscibility extends across the ternary system from the Cu-S binary boundary to the In-S binary boundary. The liquidus isothermal projection for this system was also presented.

The growth of large $CuInS_2$ single crystals was shown to be facilitated by growth under elevated pressures. Under different temperature gradients different morphologies could be obtained. Under moderate temperature gradients large single crystals were found, but with an increase in steepness of the temperature gradient a sheet-like or lamellae structure was obtained. The layers could be cleaved to a thickness of 10 μm.

Acknowledgment

The authors are grateful to M. Birkholz, Dr. Fiechter, A. Hartmann, H. Hoffmann, C. Höpfner, and Dr. Lempfuhl for discussions and assistance in some of the experimental procedures. This project was in part supported by BMFT grant number 032-9032-B.

Manuscript submitted July 19, 1991; revised manuscript received September 27, 1991. This was Paper 806 presented at the Seattle, Washington, Meeting of the Society, October 14-19, 1990.

The Hahn-Meitner-Institut assisted in meeting the publication costs of this article.

REFERENCES

1. D. Cahen and Y. Mirovsky, *J. Phys. Chem.*, **89,** 2818 (1985).
2. L. L. Kazmerski and G. A. Sanborn, *J. Appl. Phys.* **48,** 3178 (1977).
3. H. J. Lewerenz, H. Goslowsky, K.-D. Husemann, and S. Fiechter, *Nature,* **321,** 687 (1986).
4. C. D. Lokhande, *J. Power Sources,* **21,** 59 (1987).
5. K. W. Mitchell, G. A. Pollock and A. V. Mason, *Proceedings IEEE,* **1542** (1988).
6. M. Robbins *et al., This Journal,* **125,** 832 (1978).
7. P. R. Ram, R. Thanggaraj, A. K. Sharma, and O. P. Agnihotri, *Solar Cells,* **14,** 123 (1985).
8. M. A. Russak and C. J. Creter, *This Journal,* **132,** 1741 (1985).
9. B. Tell and F. A. Thiel, *J. Appl. Phys.*, **50,** 5045 (1979).
10. A. N. Tiwari, D. K. Pandya, and K. L. Chopra, *Solar Cells,* **22,** 263 (1987).
11. A. Venkatarathnam and G. V. S. Rao, *Mat. Chem. Phys.*, **16,** 145 (1987).
12. L. L. Kazmerski, "Copper-Ternary Thin-Film Solar Cells," University of Maine at Orono (1977).
13. L. L. Kazmerski, *Il Nuovo Cimento,* **2,** 2013 (1983).
14. L. L. Kazmerski and S. Wagner, in "Current Topics in Photovoltaics," T. J. Coutts and J. D. Meakin, Editors, p. 41, Academic Press, London (1985).
15. L. L. Kazmerski, F. R. White, M. S. Ayyagari, Y. J. Juang, and R. P. Patterson, *J. Vac. Sci. Technol.*, **14,** 65 (1977).
16. J. J. Loferski, *J. Appl. Phys.*, **27,** 777 (1956).

17. P. R. Subramanian and D. E. Laughlin, *Bull. Alloy Phase Diagrams*, **10,** 554 (1989).
18. D. J. Chakrabarti and D. E. Laughlin, *Bull. Alloy Phase Diagrams*, **4,** 254 (1983).
19. T. Gödecke and K. Schubert, *Z. Metallkde.*, **76,** 358 (1985).
20. J. J. M. Binsma, L. J. Giling, and J. Bloem, *J. Crystal Growth*, **50,** 429 (1980).
21. F. A. Thiel, *This Journal*, **129,** 1570 (1982).
22. M. Brüssler, H. Metzner, K.-D. Husemann, and H. J. Lewerenz, *Phys. Rev. B*, **38,** 9268 (1988).
23. H. Metzner, M. Brüssler, K.-D. Husemann, and H. J. Lewerenz, *ibid.*, In press (1991).
24. S. Mora, N. Romeo, and L. Tarricone, *Solid State Comm.*, **29,** 155 (1979).
25. R. Scheer, M. Wilhelm, and H. J. Lewerenz, *J. Appl. Phys.*, **66,** 5412 (1989).
26. M. L. Fearheiley and K. J. Bachmann, in "Materials and New Processing Technologies for Photovoltaics," J. Amick, V. Kapur, and J. Dietl, Editors, PV 83-11, p. 469, The Electrochemical Society Softbound Proceedings Series, Pennington, NJ (1983).
27. M. L. Fearheiley, N. Dietz, M. Birkholz, and C. Höpfner, *J. Electronic Mat.*, **20,** 175 (1991).
28. M. Sander, W. Jaegermann, and H. J. Lewerenz, *J. Phys. Chem.*, In press (1991).
29. M. Sander, H.-J. Lewerenz, W. Jaegermann, and D. Schmeißer, *Ber. Bunsenges. Phys. Chem.*, **91,** 416 (1987).
30. L. C. Bobb, H. Holloway, K. H. Maxwell, and E. Zimmerman, *J. Phys. Chem. Solids*, **27,** 1679 (1966).
31. N. Dietz and W. Jaegermann, Unpublished results (1990).
32. H. Goslowsky, S. Fiechter, R. Könenkamp, and H. J. Lewerenz, *Solar Energy Mater.*, **13,** 221 (1986).
33. H. J. Lewerenz, K.-D. Husemann, M. Kunst, H. Goslowsky, S. Fiechter, and H. Neff, *Mater. Lett.*, **4,** 198 (1986).
34. J. J. M. Binsma, L. J. Giling, and J. Bloem, *J. Lumin.*, **27,** 35 (1982).
35. J. J. M. Binsma, L. J. Giling, and J. Bloem, *ibid.*, 55 (1982).

Reprinted from JOURNAL OF THE ELECTROCHEMICAL SOCIETY
Vol. 139, No. 2, February 1992
Printed in U.S.A.